INT. J. NUM. METH. HEAT FLUID FLOW, VOL. 5, 601–614 (1995)

CONVECTIVE HEAT TRANSFER IN AN ANNULAR FLUID LAYER WITH CENTRIFUGAL FORCE FIELD

K. ABOUBI, L. ROBILLARD, E. BILGEN AND P. VASSEUR

Ecole Polytechnique, University of Montreal, Box 6079, Station "Centre-Ville", Montreal, Quebec, Canada, H3C 3A7

ABSTRACT

The present study deals with two-dimensional convective motion due to the effect of a centrifugal force field on a fluid contained between two horizontal concentric cylinders, for the particular case of an adiabatic inner boundary (zero heat flux) and a constant heat flux imposed on the outer boundary. The normal terrestrial gravity is considered negligible. Governing equations for a two-dimensional flow field are solved using analytical and numerical techniques. Based on a concentric flow approximation, the analytical solution is obtained in terms of the Rayleigh number and the radius ratio. The numerical solution is based on a finite difference method. Results indicate that the flow field always consists of two symmetrical cells at incipient convection even at radius ratios near unity. A good agreement is found between the analytical and numerical solutions at finite amplitude convection.

KEY WORDS Finite difference Heat transfer Natural convection Centrifugal force Annular geometry

NOMENCLATURE

k	thermal conductivity of the fluid, [$Wm^{-1} K^{-1}$]
p	dimensionless pressure
Pr	Prandtl number, ν/α
R	radius ratio, r'_2/r'_1
Ra	Rayleigh number based on the inner radius r'_1, $\beta\Omega'^2 r'^5_1 q'/\nu\alpha k$
Ra^*	Rayleigh number based on the gap between the inner and the outer radii, $Ra(R-1)^4$
Ra_c	critical Rayleigh number
Re	rotational Reynolds number, $\Omega' r'^1_1/\nu$
r	dimensionless radial coordinate
S	dimensionless sink
t	dimensionless time
T	time independent dimensionless temperature
ΔT	characteristic temperature difference
u	dimensionless velocity in r-direction
v	dimensionless velocity in φ-direction

Greek symbols

α	thermal diffusivity of the fluid, $(k/(\rho c)_f)$ [$m^2 s^{-1}$]
β	thermal expansion coefficient of the fluid, [K^{-1}]
μ	dynamic viscosity of the fluid, [$kgm^{-1} s^{-1}$]
ν	kinematic viscosity of the fluid, [$m^2 s^{-1}$]
ρ	density of the fluid, [$kg m^{-3}$]
$(\rho c)_f$	heat capacity of the fluid, [$J m^{-3} K^{-1}$]
φ	angular coordinate
Ψ	dimensionless stream function
Ω	angular velocity [s^{-1}]
ω	dimensionless vorticity

Superscripts

$'$	dimensional variable
$*$	refers to physical time dependent temperature

0961–5539/95/070601–14$2.00

Received February 1994
Revised May 1994

Subscripts

1 value on inner cylinder
2 value on outer cylinder

Other symbols

∇^2 Laplacian operator, $\left(\nabla^2 = \frac{1}{r}\frac{\partial}{\partial r}\left(r\frac{\partial}{\partial r}\right) + \frac{1}{r^2}\frac{\partial^2}{\partial \varphi^2}\right)$

INTRODUCTION

Natural convection in rotating fluids has been the subject of many investigations due to its diverse applications ranging from large scale systems found in meteorology, oceanography and astrophysics[1] to small scale industrial devices such as those used in food industry to thermally process canned liquids[2] and in the manufacture of high quality optical waveguides[3]. The problem is also encountered in the case of rotating machinery, where the centrifugal force may become quite high. Some applications have been made by Schmidt[4], who used hollow turbine blades to increase heat transfer via centrifugally driven convection and found that rotation could augment heat transfer in water cooled turbine blades. These past studies may be classified according to the direction of the rotation axis which is either vertical, in which case the vectors of gravity and rotation do not coincide[5] or horizontal, in which case these two vectors are coplanar[2].

As mentioned by Randriamampianina *et al.*[6], who considered the vertical rotating annulus, a complex three-dimensional flow may occur from the combined effect of the terrestrial gravity, centrifugal and Coriolus forces. By contrast, two-dimensional flows are expected, according to Robillard and Torrance[7], Ladeinde and Torrance[8] and Prud'homme *et al.*[9] for long horizontal cylinders and annuli where the effects of end boundaries are negligible. However, if the horizontal cylinder is of finite length with differential heating on the two ends, then the treatment of the problem must be three-dimensional. This was done by Yang *et al.*[2].

Of course, the fundamental differences arising from the specific orientation of the rotation axis should vanish when the terrestrial gravity force becomes negligible compared to the centrifugal force. For this asymptotic limit, long cylinders and annuli will develop convective cells with their axes parallel to that rotation axis. As mentioned by Busse[10], the centrifugal force replaces gravity and the problem may be compared to the Benard convection in a layer heated from below. The general two-dimensional study undertaken by Ladeinde and Torrance[11] on rotating cylinders includes this asymptotic limit, for the case of a uniformly distributed heat sink and uniform temperature imposed on the circular boundary. It provides the critical Rayleigh number at which Benard cells will occur.

In the present investigation, the problem of convective heat transfer in an annular fluid layer under the influence of a centrifugal force field is investigated. The centrifugal force field dominates and the normal (terrestrial) gravity is considered negligible. The outer boundary is heated with a constant heat flux while the inner boundary is adiabatic (no heat loss). Under such conditions the problem is essentially a transient one, the temperature increasing continuously with time. However, the induced motion does not depend on the temperature itself, but on (spatial) temperature gradients. Those temperature gradients are expected to become time-dependent after an initial transient, giving rise to a steady state flow field identical to the one that would be obtained at constant (time independent) temperature, if a uniformly distributed heat sink was imposed between the two boundaries. A two-dimensional simulation in (r, φ) coordinates of the annulus is carried out. The problem is studied numerically by using a finite difference method and also analytically using a "concentric" flow assumption similar to the parallel flow approach used by Sen *et al.*[12] for an elongated cavity. Effects of various parameters, such as the Rayleigh number and the radius ratio, are examined and comparisons between numerical and analytical results are presented.

STATEMENT OF THE PROBLEM

The problem is solved in a non inertial coordinate system rotating along with the enclosure at constant angular velocity Ω', as shown in *Figure 1*. The inner boundary of radius r'_1 is assumed to be perfectly insulated (adiabatic conditions). A uniform heat flux $q' = -k\dfrac{\partial T'^*}{\partial r'}$ is imposed on the outer boundary of radius r'_2. Fluid properties are taken to be constant except the density of the fluid for which the validity of the Oberbeck-Boussinesq approximation is assumed. The governing equations in the rotating frame are obtained from the theory of rotating flows[13].

Introducing the dimensionless variables:

$$\left.\begin{aligned} r &= r'/r'_1, & (u, v) &= (u', v')/(r'_1/\alpha) \\ t &= \alpha t'/r'^2_1, & p &= p'_d r'^2_1/\rho_1 \alpha^2 \\ \omega &= \omega' r'^2_1/\alpha, & \Psi &= \Psi'/\alpha \\ T^* &= (T'^* - T'^*_1)/\Delta T', & R &= r'_2/r'_1 \\ & & \Delta T' &= q' r'_1/k \end{aligned}\right\} \tag{1}$$

where T'^*_1 is a reference temperature chosen at $r' = r'_1$ and $\varphi = 0$. ρ_1 is the density corresponding to T'^*_1, $\Delta T'$ is a characteristic temperature and $p'_d = p' - \rho_1 \Omega^2 r'^2/2$ is the dynamic pressure. Other symbols are defined in the nomenclature.

The governing equations in dimensionless form are:

$$\nabla \cdot \vec{V} = 0 \tag{2}$$

$$\frac{D\vec{V}}{Dt} + 2Re\, Pr \hat{z} \times \vec{V} = -\nabla p + Pr\, \nabla^2 \vec{V} + Pr\, Ra T^* \hat{r} \tag{3}$$

$$\frac{DT^*}{Dt} = \nabla^2 T^* \tag{4}$$

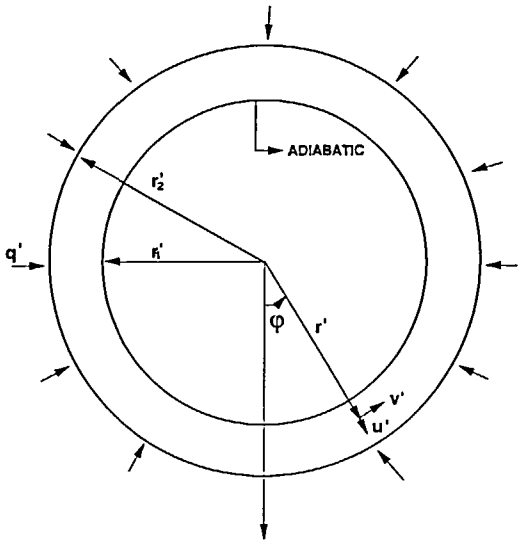

Figure 1 Geometry of the problem

where $\hat{r}$ and $\hat{z}$ are unit vectors in the radial and axial directions, respectively. $Ra = \beta\Omega'^2 r_1'^5 q'/\nu\alpha k$ is the Rayleigh number based on the constant heat flux and the centrifugal force field, $Pr = \nu/\alpha$ is the Prandtl number and $Re = \Omega r_1'^2/\nu$ is the rotational Reynolds number. For $R \to 1$, it is more appropriate to use a modified Rayleigh number based on the gap $r_2' - r_1'$, $Ra^* = Ra(R-1)^4$. The second term on the left hand side of (3) is the Coriolis term which has, in fact, no dynamic effect within the two-dimensional framework considered here.

With the present thermal boundary conditions, the temperature at every point will increase continuously with time. However, as mentioned earlier, the temperature gradients are expected to become time independent after an initial transient. Since the flow field depends on temperature gradients, it should reach a steady state. When this steady state is reached, the temperature itself increases linearly with time at the same rate for every point in the flow domain. As described by Robillard and Vasseur[14], the temperature may then be re-defined as $T^* = T + St$ so that its asymptotic time dependence is treated in a separate term. Equation (4) becomes:

$$\frac{DT}{Dt} = \nabla^2 T + S \tag{5}$$

where S acts as fictitious dimensionless source term uniformly distributed over the flow domain. This source term must compensate for the incoming heat from the outer boundary, i.e. $S = 2R/(R^2 - 1)$.

The temperature field satisfies the Neuman boundary conditions:

$$\left.\frac{\partial T}{\partial r}\right|_{r=1} = 0 \tag{6}$$

$$\left.\frac{\partial T}{\partial r}\right|_{r=R} = 1 \tag{7}$$

and the velocity field components satisfy the no-slip conditions. The pressure gradient and the Coriolis term are eliminated by taking the curl of (3) and the following vorticity equation is obtained:

$$\frac{D\omega}{Dt} = Pr\,\nabla^2\omega + Pr\,Ra\frac{\partial T}{\partial \varphi} \tag{8}$$

where the dimensionless vorticity is defined as:

$$\omega = \frac{1}{r}\left(\frac{\partial rv}{\partial r} - \frac{\partial u}{\partial \varphi}\right) \tag{9}$$

Velocity components and vorticity may be expressed in terms of a stream function Ψ

$$u = \frac{1}{r}\frac{\partial \Psi}{\partial \varphi}, \qquad v = -\frac{\partial \Psi}{\partial r} \tag{10}$$

$$\omega = -\nabla^2 \Psi \tag{11}$$

No net flow should exist around the annulus and consequently, the value of the stream function on the two boundaries is set to zero:

$$r = 1, R: \qquad \Psi = 0 \tag{12}$$

The no-slip boundary condition yields:

$$r = 1, R: \qquad \frac{\partial \Psi}{\partial r} = 0 \tag{13}$$

ANALYTICAL SOLUTION

For steady state conditions, a concentric flow approach analogous to the parallel flow approach for shallow cavities used by Sen *et al.*[12] and Robillard and Vasseur[14] is considered for the present problem. In the context of elongated cavities, it should be recalled that the critical Rayleigh number for incipient convection with heating from below by a constant heat flux corresponds to the occurrence of a single cell, i.e. to the lowest wave number[15]. For the present problem, one should expect one pair of convective cells at incipient convection. A schema of the expected flow is shown in *Figure 2* where in the core regions the flow is concentric, with:

$$u = 0 \tag{14}$$

$$v = v(r) \tag{15}$$

v satisfies the zero net flow condition (12), i.e.:

$$\int_1^R v dr = 0 \tag{16}$$

Therefore, in each core region, there are two layers (inner and outer) flowing in opposite directions. Those layers are connected in the "end regions" shown in *Figure 2*, where conditions given by (14) and (15) are not fulfilled.

The present analytical solution concerns the core region. Within each core region of *Figure 2*, the temperature field can be expressed as a sum of an unknown function of r and a linear function of φ. As a result, the temperature field must be of the following form:

$$T = \theta(r) + C\varphi \tag{17}$$

where C is an unknown temperature gradient in the φ direction. C is constant within one core region but changes its sign from one core region to another around the annulus. The stream

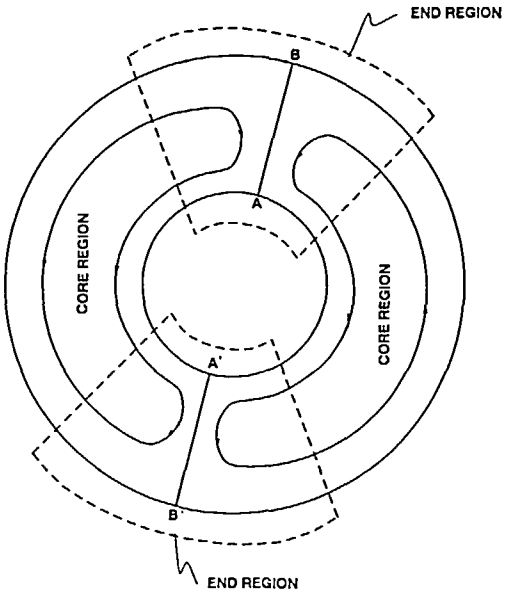

Figure 2 Schematic of the concentric flow approach

function itself depends exclusively on r:

$$\Psi = \Psi(r) \tag{18}$$

Substituting (17) into (5), replacing the vorticity in (8) by its expression (11) and considering condition given by (18), we obtain:

$$L\theta = -\frac{C}{r}\frac{\partial \Psi}{\partial r} - S \tag{19}$$

$$L^2\Psi = Ra\, C \tag{20}$$

where $L = \frac{1}{r}\frac{d}{dr}\left(r\frac{d}{dr}\right)$.

Equations (19) and (20) are solved for θ and Ψ using boundary conditions given by (6), (7), (12) and (13):

$$\theta = Ra\, C^2 Z(r) + \theta_c \tag{21}$$

and

$$\Psi = Ra\, C F(r) \tag{22}$$

where $Z(r)$ and $F(r)$ are parametric functions of the radius ratio:

$$Z(r) = -\frac{r^4}{256} - \frac{1}{8}\left(b - \frac{3}{2}a\right)r^2 - \frac{a}{8}r^2 \ln r - d \ln r - \frac{c}{2}(\ln r)^2 \tag{23}$$

$$F(r) = \frac{r^4}{64} + (b-a)\frac{r^2}{4} + \frac{a}{4}r^2 \ln r + c \ln r + d \tag{24}$$

The parameters involved in equations (23) and (24) are:

$$a = \frac{1}{8}\frac{4R^2 \ln R - (R^4 - 1)}{R^2 - 1 - 4\dfrac{R^2}{R^2 - 1}(\ln R)^2}, \qquad b = a\left(\frac{1}{2} - \frac{R^2}{R^2 - 1}\ln R\right) - \frac{R^2 + 1}{8}$$

$$c = \frac{a}{4} - \frac{b}{2} - \frac{1}{16}, \qquad d = \frac{a - b}{4} - \frac{1}{64}$$

θ_c in (21) is the pure conduction temperature field:

$$\theta_c = \frac{R}{R^2 - 1}\left(\frac{r^2 - R^2}{2} - \ln \frac{r}{R}\right) \tag{25}$$

The velocity component v is obtained from the stream function:

$$v = -Ra\, C\left(\frac{r^3}{16} + \left(b - \frac{a}{2}\right)\frac{r}{2} + \frac{a}{2}r \ln r + \frac{c}{r}\right) \tag{26}$$

An additional constraint lies in the fact that the heat transported across any transversal section should be zero so that:

$$\int_1^R \left(vT - \frac{1}{r}\frac{\partial T}{\partial \varphi}\right) \mathrm{d}r = 0 \tag{27}$$

using equations (26) and (17) for v and T respectively, we obtain from (27):

$$C = -\frac{1}{\ln R}\int_1^R \frac{\mathrm{d}\Psi}{\mathrm{d}r}\,\theta\, \mathrm{d}r \tag{28}$$

We substitute the solutions θ and Ψ given by (21) and (22) into (28) and integrate to get:

$$Ra^2C^3I_1 + Ra\,CI_2 + C = 0 \tag{29}$$

where

$$\left.\begin{aligned} I_1 &= \frac{1}{\ln R}\int_1^R F'Z\,\mathrm{d}r \\ I_2 &= -\frac{1}{\ln R}\int_1^R F'\theta_c\,\mathrm{d}r \end{aligned}\right\} \tag{30}$$

The non-trivial solutions of (29) are:

$$C = \pm\frac{1}{Ra}\sqrt{\frac{Ra\,I_2 - 1}{I_1}} \tag{31}$$

Since I_1 is a positive quantity, C is real provided that $Ra > -1/I_2$, where I_2 is a negative quantity. The onset of convection corresponds to:

$$Ra = Ra_c = \frac{1}{I_2} \tag{32}$$

A Nusselt number for the core region may be defined as:

$$Nu = \frac{\Delta\theta_c}{\Delta\theta} \tag{33}$$

where $\Delta\theta = \theta(R) - \theta(1)$ is the dimensionless temperature difference. ΔT_c stands for the pure conduction regime. From (21), (23) and (25), we obtain:

$$Nu = \left[1 + \frac{Ra\,C^2[Z(R) - Z(1)]}{R\left(\frac{1}{2} - \frac{\ln R}{R^2 - 1}\right)}\right]^{-1} \tag{34}$$

NUMERICAL STUDY

The numerical computations are carried out using standard finite difference methods. The governing equations (5) and (8) for temperature and vorticity are solved with an alternating direction implicit method (A.D.I.). A successive overrelaxation method is used to solve the Poisson equation (11) for the stream function. All derivatives are discretized according to the Taylor-based second order central difference scheme for a regular mesh size. The A.D.I. approach in the φ direction is based on the fact that any physical variable f should satisfy periodic conditions of the form:

$$f(r, \varphi) = f(r, \varphi + 2\pi) \tag{35}$$

With periodic boundary conditions in the φ-direction, the resulting matrix is no more tridiagonal. However, it is possible, by a matrix partition procedure, to bring back the problem to the solution of tridiagonal matrices for which efficient recurrence formula such as the Thomas algorithm are available. More details about the partition technique may be found in Phillips' work[16]. The boundary values for the vorticity at $r = 1, R$ are obtained by performing power series expansion in Δr of the stream function and expressing the derivatives of Ψ in terms of the vorticity. The results presented are obtained using a grid size of 18 × 36 corresponding to the r–φ directions. To examine the influence of grid size on the flow field, some cases with $R = 1.5$

were also calculated with a 36×72 grid size. Flow and temperature fields were practically identical to the results obtained with the 18×36 grid size for the Rayleigh number Ra as large as 10^7 ($Ra^* \simeq 625000$). The nonlinear coupled equations (2) to (4) are solved iteratively with a time step of 5×10^{-5} for small Rayleigh numbers and radius ratios and 2×10^{-5} for high Rayleigh numbers and radius ratios.

RESULTS AND DISCUSSION

In this section, numerical results are compared with the analytical results from the concentric flow approach. Numerical solutions are obtained for $Pr = 1$ and for the ranges $Ra_c < Ra < 10^7$ and $1 < R < 2.5$. As mentioned earlier, the numerical solution of governing equations (5), (8) and (11) starts from initial conditions with transient flow (Ψ) and temperature (T) fields evolving towards a final steady state. The following discussion deals with steady-state results. Also it must be mentioned that the choice of a given Prandtl number for the numerical solution is of no consequence in the comparison of the numerical results with the analytical approach since this latter concerns the core region (see *Figure 2*) where no inertia effects are present. However, at values of Pr much below unity, inertia effects of the end regions become important and conditions given by (14), (15) and (16) cannot be fulfilled.

The pure conduction temperature field for this particular problem produces a stable rest state with concentric isotherms perpendicular to the force field. Motion will occur only beyond a given threshold in terms of a critical Rayleigh number Ra_c. This critical Rayleigh number may be predicted analytically with the hypothesis of the concentric flow which leads to equation (32). *Figure 3* gives $Ra_c^* = Ra_c(R-1)^4$ as a function of the aspect ratio R. The value $Ra_c^* = 1440$ for $R \to 1$ corresponds to the limit case of a horizontal layer subjected to a normal gravity field. This case was treated in the past by Kulacki and Goldstein[17] for which a value $Ra_c = 1440$ was obtained and more recently by Vasseur and Robillard[18].

In a manner analogous to the parallel flow hypothesis for the shallow cavity (see for instance Sen *et al.*[19]), results obtained in the present analytical framework are valid provided that the radial velocity component u is vanishingly small over a finite range of the coordinate φ, i.e., provided that the core regions of *Figure 2* have a finite extent.

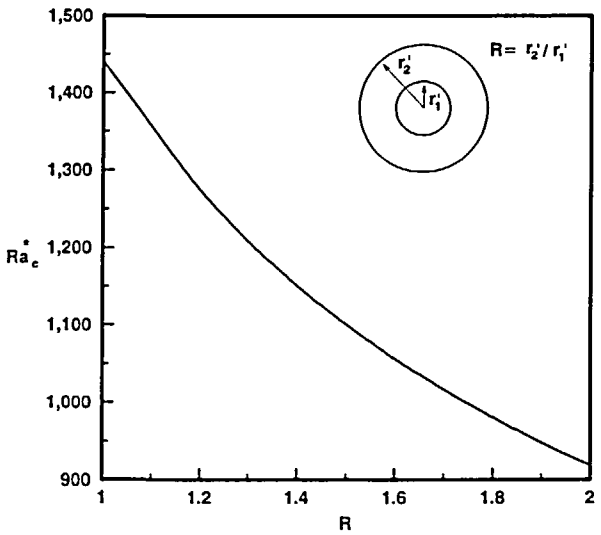

Figure 3 Critical Rayleigh number Ra_c^* based on the gap $(r_2' - r_1')$ as a function of the radius R

At a given radius ratio, this condition is best fulfilled when there are only two end regions (or equivalently two convective cells) around the annulus. End regions are required to connect together in a closed loop the inner and outer flows which circulate in opposite φ directions within the core region and, consequently, there cannot be less than two convective cells around the annulus.

Unstable layers with thermal boundary conditions of the Neuman type are characterized by incipient convection corresponding to the lowest wavenumber compatible with the geometry considered. In the present case, we expect the first convective motion beyond the threshold given in *Figure 3* to contain two convective cells. Numerical tests were conducted at $R = 2$ for Ra values slightly above $Ra_c = 920$. The numerical computations were started from initial conditions corresponding to a motionless fluid with a pure conduction temperature field. With those conditions, two-cell flow patterns were indeed obtained for $Ra < 1100$. For $Ra > 1100$ four-cell flow patterns did occur. Such a behaviour is not surprising since the threshold for the occurrence of flow configurations with twice the number of cells follows quite closely the lowest threshold given in *Figure 3*. Nevertheless, a stable two-cell flow pattern can be obtained at relatively high Ra if the numerical computation starts from initial conditions containing two cells.

Flow and temperature fields obtained numerically for the same radius ratio $R = 1.5$ but for three different Rayleigh numbers $Ra = 1.9 \times 10^4$, 2.8×10^4 and 10^5 ($Ra^* = 1187.5$, 1750 and 6250) are shown in *Figure 4*. These flow and temperature fields are represented by streamlines (left) and isotherms (right), respectively. Each set contains two cells and was obtained by starting the numerical computation from initial conditions containing two cells. It is seen that for each of the three cases the convective cells are symmetric with respect to a diameter oriented vertically on the figure. However, there is no preferred position in the φ direction and the horizontal isotropy characterizing the Benard cells in a fluid layer of infinite extent becomes a "circular isotropy" for the present problem. The case shown in *Figure 4a* is slightly above the critical Rayleigh number $Ra_c^* = 1100.87$, value obtained from the concentric flow analysis for a radius ratio $R = 1.5$. The regime is pseudo-conductive with a weak departure of the isotherms from the concentric configuration. With increasing Ra^*, the distortion of isotherms is amplified but the two-cells pattern can be maintained, as it can be seen in *Figures 4b, c*. However, at much higher Rayleigh numbers it was found (not shown here) that this flow field was broken and multi-cells were produced.

A flow field with four cells such as the one shown in *Figure 5a* can be obtained numerically by using initial conditions containing four cells. It is even possible to obtain a flow pattern containing more cells by using appropriate initial conditions.

It is observed in *Figure 5a* that the conditions given by (14) and (15) are not fulfilled over a finite range of the coordinate φ. This means that the concentric flow approach is not appropriate to describe the actual flow field. The same inadequacy occurs when the radius ratio is increased. For instance, the flow field with $R = 2.5$ and $Ra = 1000$ ($Ra^* = 5062.5$) shown in *Figure 5b*, has a much reduced core region, by comparison to the cases shown in *Figures 4a, b, c*. Therefore, results from the concentric flow analysis are restricted to radius ratio not too far from unity.

Results from the numerical calculations are compared with the analytical solution using the concentric flow assumption in *Figures 6, 7* and *8*. They show, respectively, the extremum values of the stream function Ψ_E, the Nusselt number Nu, as defined by (34) and some azimuthal velocity distributions. All numerical results in these figures involve two-cell flow configurations and are taken at a cross-section midway between end regions. Ψ_E and Nu are given as functions of the Rayleigh number Ra^* for radius ratios varying from 1.2 to 2.5. It is observed in *Figure 6* that the agreement between numerical results and analytical predictions is good for the range of Rayleigh numbers considered; this is true even at aspect ratios of 2.5. Each of the analytical curves starts at a critical Rayleigh number $Ra_c^* = Ra_c(R-1)^4$, where Ra_c is given by (32). Numerical results at increasing Rayleigh numbers were obtained step by step using as initial conditions the previous results at lower Rayleigh numbers. This process is pursued until the two-cell flow breaks into a multi-cell pattern.

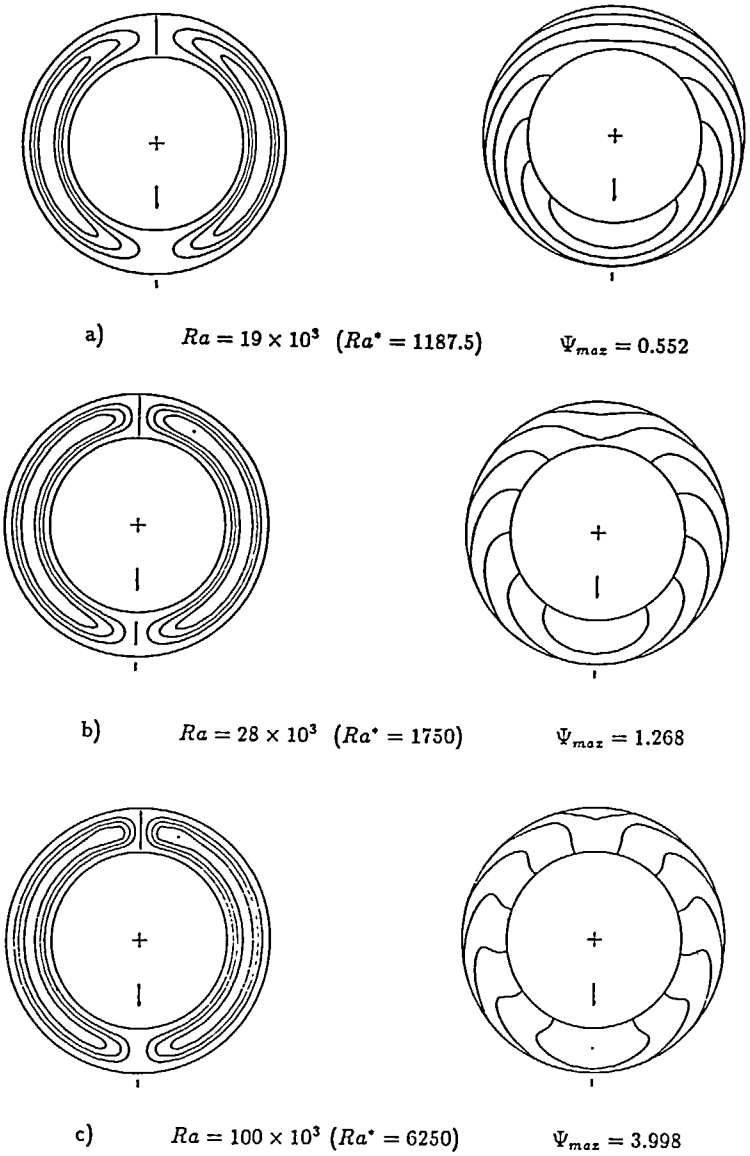

Figure 4 Flows and temperature fields containing two cells at different Rayleigh numbers, for $R = 1.5$. The flow and temperature fields are shown by streamlines (left) and isotherms (right) respectively

In *Figure 7*, it is seen that the effect of the radius ratio on the Nusselt number is less important than the one observed in *Figure 6*, i.e., the curves corresponding to different R are closely spaced. The ordering of the numerical results follows the analytical predictions. However, with increasing Rayleigh number, there is a tendency for the numerical values to be above the analytical curves. With the Rayleigh number increasing further to very large values, the Nusselt number, as predicted by the concentric flow analysis reaches an asymptotic value function of the radius ratio. Practically, however, this prediction does not hold since the flow breaks into many cells at Rayleigh numbers much below this asymptotic limit.

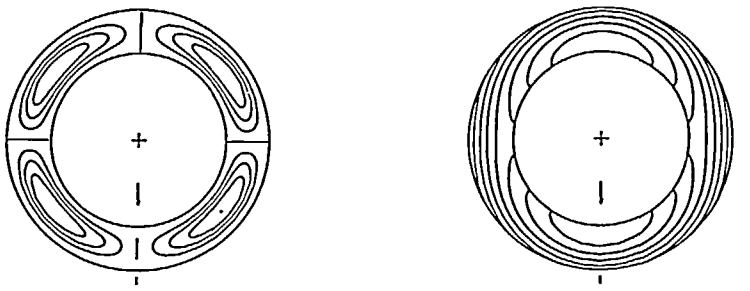

a) $R = 1.5$ $Ra = 19 \times 10^3$ $(Ra^* = 1187.5)$ $\Psi_{max} = 0.510$

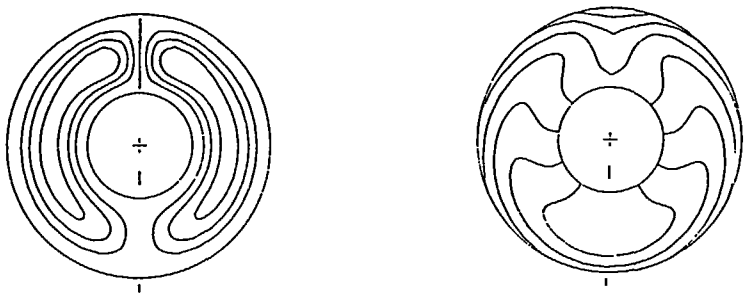

b) $R = 2.5$ $Ra = 10^3$ $(Ra^* = 5062.5)$ $\Psi_{max} = 4.375$

Figure 5 Four-cell patterns. The flow and temperature fields are shown by steamlines (left) and isotherms (right) respectively

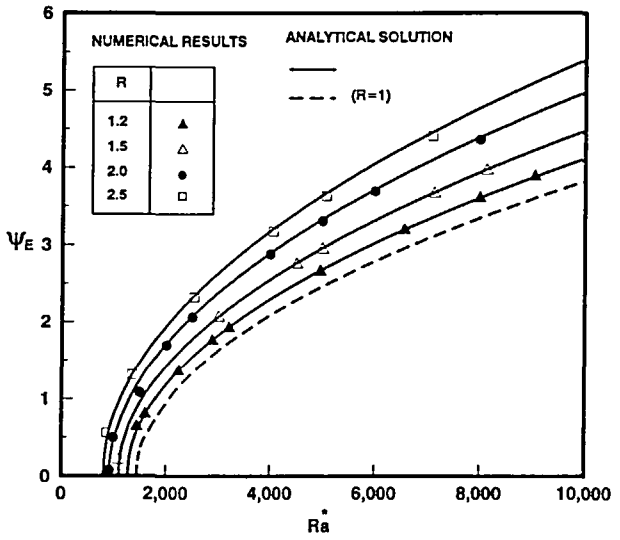

Figure 6 Extremum value of stream function Ψ_E as a function of the Rayleigh number

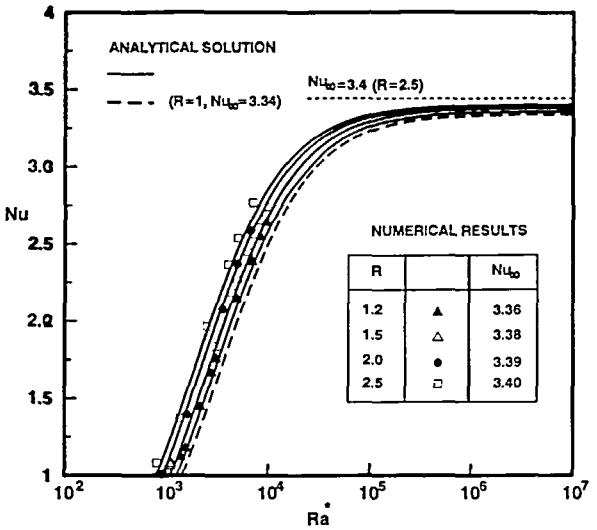

Figure 7 Nusselt number Nu as a function of the Rayleigh number Ra^*

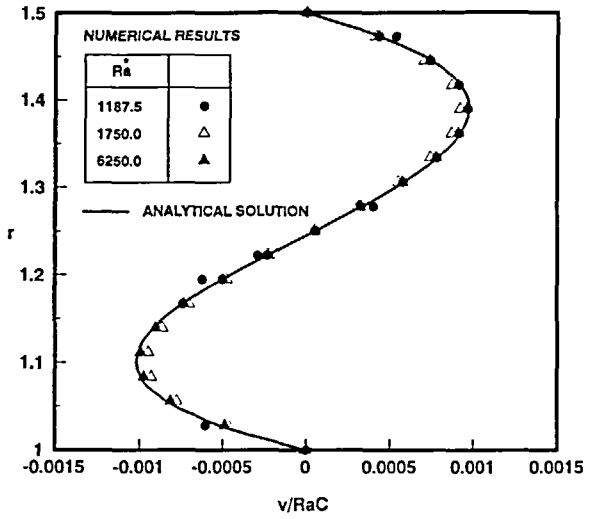

Figure 8 Azimuthal velocity distribution v as a function of r ($R = 1.5$)

The non-dimensional velocity v in the φ direction is given in *Figure 8* as a function of the radius r for the three Rayleigh numbers of *Figure 4* ($Ra^* = 1187.5$, 1750 and 6250) and for the radius ratio $R = 1.5$ of *Figure 4a, b, c*. In order to present a single analytical curve, analytical and numerical results for v are divided by $Ra\,C$ where C is the theoretical temperature gradient obtained from equation (28). It is seen that the numerical results agree in a satisfactory way with the analytical prediction.

CONCLUSIONS

Natural convection in a fluid contained between two horizontal concentric cylinders has been investigated both analytically and numerically for the case of an adiabatic inner boundary and a constant heat flux imposed on the outer boundary in the presence of a centrifugal force field. An analytical approach, based on a concentric flow assumption transforms the governing equations into ordinary differential equations. The critical Rayleigh number for the onset of convection is predicted by this approach. Moreover at finite amplitude convection, this approach predicts the flow and temperature fields within the core region. A numerical simulation of the full governing equations has also been performed for the range $Ra_c < Ra < 10^6$. A good agreement is found between the concentric flow analytical approach and the numerical simulation for radius ratio <3.0. It is found from the numerical simulation that the flow pattern near the critical Rayleigh consists of two cells even if the radius ratio is near unity. However, additional pairs of cells are possible when the Rayleigh number is increased from the critical value.

ACKNOWLEDGEMENT

Financial support by Natural Sciences and Engineering Research Council of Canada and FCAR of Province of Quebec are acknowledged.

REFERENCES

1 Hide, R. and Mason, P. J. Baroclinic waves in a rotating fluid subject to internal heating, *Phil. Trans. R. Soc. Lond.*, **268**, 201–232 (1970)
2 Yang, H. Q., Yang, K. T. and Lloyd, J. R. Rotational effects on natural convection in a horizontal cylinder, *A.I.C.H.E. J.*, **34**, 1627–1633 (1988)
3 Lin, Y. T., Choi, M. and Greif, R. A three-dimensional analysis of particle deposition for the modified chemical vapor deposition (MCVD) process, *J. Heat Transfer*, **114**, 735–742 (1992)
4 Schmidt, E. H. W. Heat transmission by natural convection at high centrifugal acceleration in water-cooled gas-turbine blades, in *I.M.E. A.S.M.E. General Discussion on Heat Transfer*, 361–363 (1951)
5 Or, A. C. and Busse, F. H. Convection in a rotating cylindrical annulus. Part 2 Transitions to asymmetric and vacillating flow, *J. Fluid Mech.*, **174**, 313–326 (1987)
6 Randriamampianina, A., Bontroux, P. and Roux, B. Ecoulements induits par la force gravifique dans une cavité cylindrique en rotation, *Int. J. Heat Mass Transfer*, **30**, 1275–1292 (1987)
7 Robillard, L. and Torrance, K. E. Convective heat transfer inhibition in an annular porous layer rotating at weak angular velocity, *Int. J. Heat Mass Transfer*, **33**, 953–963 (1990)
8 Ladeinde, F. and Torrance, K. E. Galerkin finite element simulation of convection driven by rotation and gravitation, *Int. J. Num. Meth. Fluids*, **10**, 47–77 (1990)
9 Prud'homme, M., Robillard, L. and Hilal, M. Natural convection in an annular fluid layer rotating at weak angular velocity, *Int. J. Heat Mass Transfer*, **36**, 1529–1539 (1993)
10 Busse, F.H. Thermal instabilities in rapidly rotating systems, *J. Fluid Mech.*, **44**, 441–460 (1970)
11 Ladeinde, F. and Torrance, K. E. Convection in rotating horizontal cylinder with radial and normal gravity forces, *J. Fluid Mech.*, **228**, 361–385 (1991)
12 Sen, M., Vasseur, P. and Robillard, L. Parallel flow convection in a tilted two-dimensional porous layer heated from all sides, *Phys. Fluids*, **31**, 3480–3487 (1988)
13 Greenspan, H. P. *The Theory of Rotating Fluids*, Cambridge University Press (1969)
14 Robillard, L. and Vasseur, P. Quasi-steady state natural convection in a tilted porous layer, *Can. J. Chem. Eng.*, **70**, 94–100 (1992)
15 Nield, D. A. Onset of thermohaline convection in a porous medium, *Water Resources Res.*, **4**, 535–560 (1968)
16 Phillips, W. R. C. *The Generalized Lagrangian Mean Equations and Streamwide Vortices, Near Wall Turbulence* (Ed. S. Kline), Hemisphere (1988)
17 Kulacki, F. A. and Goldstein, R. J. Hydrodynamic instability in fluid layers with uniform volumetric energy sources, *Appl. Sci. Res.*, **31**, 81–109 (1975)
18 Vasseur, P. and Robillard, L. The Brinkman model for natural convection in a porous layer: effects of nonuniform gradient, *Int. J. Heat Mass Transfer*, in press (1994)
19 Sen, M., Vasseur, P. and Robillard, L. Multiple steady states for unicellular natural convection in an inclined porous layer, *Int. J. Heat Mass Transfer*, **30**, 2097–2113 (1987)

APPENDIX

The value of I_1 and I_2 in (30), are given by the following expressions:

$$I_1 = \frac{1}{\ln R}\{b_1(R^8-1) + b_3(R^6-1) + b_4(R^4-1) + b_5(R^2-1) + b_6R^6 \ln R + b_7R^4 \ln R + b_8R^2 \ln R + b_9R^4(\ln R)^2 + b_{10}R^2(\ln R)^2 + b_{11}(\ln R)^2 + b_{12}R^2(\ln R)^3 + b_{13}(\ln R)^3\}$$

$$I_2 = \frac{R}{\ln R}\{a_1 + a_2(R^2+1) + a_3(R^4+R^2+1)\} + a_4R^5/R^2 - 1 + a_5R^3/R^2 - 1 + a_6 \ln R/R^2 - 1$$

where the coefficients a_i and b_i, are:

$a_1 = (4c + 2b - 3a)/16$ $\quad b_4 = [a(-a - b_2 + b) - 4b_2b + d]/256$

$a_2 = (16b - 12a + 1)/256$ $\quad b_5 = -(2cb_2 - 2(2d - c)b + (c + 6d)a)/32$

$a_3 = 1/192$ $\quad b_6 = -5a/3072$

$a_4 = (4a - 1)/64$ $\quad b_7 = (4a(a - b_2 - b) + c - 4d)/256$

$a_5 = (3a - 2b)/8$ $\quad b_8 = -(a(5c - 6d) + b(4d - 2c))/16$

$a_6 = -R(aR^2 + 2c)/4$ $\quad b_9 = -(a^2 + c/2)/64$

$b_1 = -1/32768$ $\quad b_{10} = -(2a(d - c) + cb)/8$

$b_2 = b - 3a/2$ $\quad b_{11} = -cd/2$

$b_3 = (17a/2 - 5b)/3072$ $\quad b_{12} = -ca/8$ $\quad b_{13} = -c^2/6$